The Anti-Microbial Activity of Titania-Nickel Ferrite Composite Nanoparticles

S. Rana and R.D.K. Misra

A novel approach to synthesize a new generation of composite nanoparticles consisting of a photocatalytic shell of anatase-titania and a magnetic core of nickel ferrite has been adopted combining reverse micelle and chemical hydrolysis techniques. Titania is an effective anti-microbial agent that can be directly sprayed on infected areas of the human body or environment. Unfortunately, titania is an electrical insulator and is difficult to extract from the sprayed surface after treatment. The titania photocatalytic shell provides good anti-microbial capability that renders the bacteria inactive and removes the organic pollutants, while the nickel ferrite magnetic core enables controlled delivery of composite nanoparticles through the application of a small magnetic field, encouraging their application as removable anti-microbial photocatalyst nanoparticles.

INTRODUCTION

During the past decade various photocatalytic techniques have been investigated to address the increasing problem of environmental pollution. In this regard, the application of titania as a photocatalyst has assumed particular significance in the purification of water and air.[1–5] Titania-mediated photooxidation is promising for the elimination of microorganisms in many applications (e.g., self-cleaning and self-sterilizing applications).[6,7]

During the irradiation of TiO_2 with ultraviolet (UV) light, a UV photon is absorbed by a TiO_2 particle, and an electron (e^-)-hole (h^+) pair is generated. The e^- and h^+ may migrate to the surface of the photocatalyst particle and react with adsorbed reactants resulting in the desired process, or they may undergo undesired recombination.[8] In the presence of water/oxygen, the redox reaction produces hydroxyl radicals that oxidize pollutants or can be used as anti-microbial agents.[9,10]

TiO_2 particles are electrical insulators and are difficult to extract from the sprayed surface after treatment. However, their removal can be facilitated by synthesizing composite particles consisting of a magnetic core and a photocatalytic shell. A number of attempts have been made in recent years to design magnetic core-photocatalytic shell structures.[11–14] However, the efforts to utilize the core-shell structures as photocatalyst materials for anti-microbial and water purification systems are limited. Separable magnetic titania catalysts are generally processed by the sol-gel or solid-reaction method, resulting in an

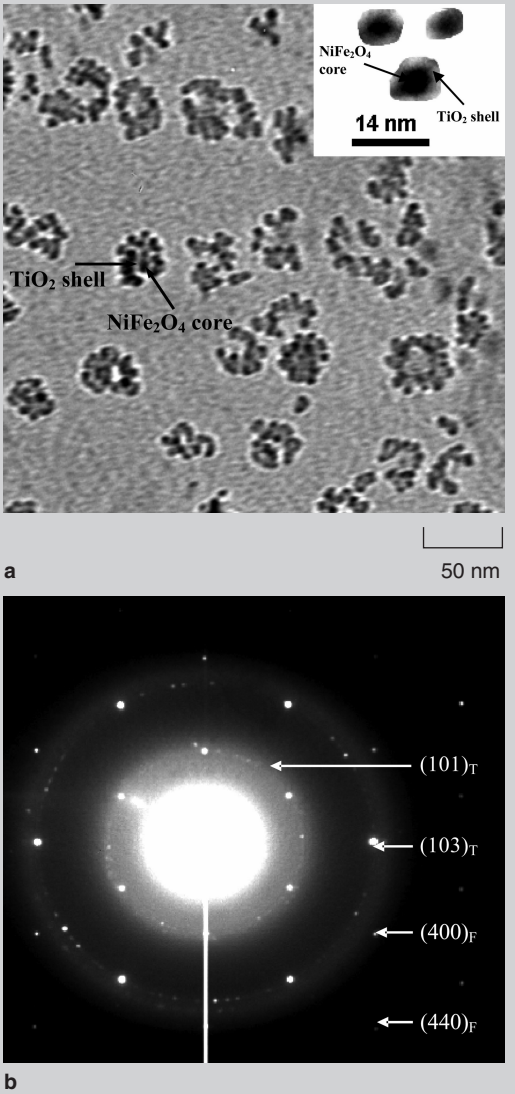

Figure 1. (a) A high-magnification TEM micrograph of the core-shell structure for TiO_2-$NiFe_2O_4$ composite nanoparticles, illustrating the core-shell structure in the inset and (b) an electron diffraction pattern for TiO_2-$NiFe_2O_4$.

amorphous titania. Thus, heat treatment leading to the crystallization of the hydrous TiO_2 into a photoactive material is essential in the synthesis of a photocatalytic material. An alternative method that eliminates heat treatment is required. In this study, crystalline TiO_2 is directly coated as a shell onto a magnetic core. To accomplish this objective, a process was developed that uniquely combines the reverse micelle technique and a chemical precipitation process to synthesize composite nanoparticles consisting of a photocatalytic shell of anatase-titania and a magnetic core of nickel ferrite. This article describes the antimicrobial activity of the composite nanoparticles with particular reference to E. coli bacteria because it is commonly used as a biological indicator of disinfection efficiency in water systems.

See the sidebar for experimental procedures.

RESULTS AND DISCUSSION

Structural Characterization of TiO_2-$NiFe_2O_4$ Composite Nanoparticles

A representative high-magnification transmission-electron-microscope (TEM) image of TiO_2-$NiFe_2O_4$ composite nanoparticles is presented in Figure 1a. The direct coating of titania onto the surface of the magnetic nickel ferrite particles resulted in a core-shell structure in which the $NiFe_2O_4$ was predominantly concentrated in the center of the composite nanoparticles. The micrograph in Figure 1a illustrates the composite nature of particles consisting of a dark $NiFe_2O_4$ magnetic core and a gray TiO_2 shell. The $NiFe_2O_4$ magnetic core is ~4–6 nm and the TiO_2 shell ~2–3 nm. The electron diffraction pattern obtained for the nanoparticles (Figure 1b) consists of four resolved concentric rings. In the figure, the letters F and T relate to ferrite and titania, respectively. The (400) and (440) reflections correspond to spinel nickel ferrite, while (101) and (103) reflections correspond to anatase-titania. The d-values obtained from the diffraction pattern for nickel ferrite and titania (nickel ferrite: d = 0.2062 nm for (400) and d = 0.1473 nm for (440) reflections; anatase-titania: d = 0.3520 nm for (101) and d = 0.2366 nm for (103) reflections) compared well with the d-values measured from the x-ray diffraction data. A summary of the x-ray diffraction data for the TiO_2-$NiFe_2O_4$ composite nanoparticles is presented in Table I. The table compares the x-ray diffraction peak positions for TiO_2-$NiFe_2O_4$ composite nanoparticles with standard $NiFe_2O_4$ and anatase-phase of TiO_2. The experimental data is consistent with nickel ferrite and anatase-titania.

EXPERIMENTAL PROCEDURES

Synthesis of TiO_2-$NiFe_2O_4$ Composite Nanoparticles

In this study, nickel ferrite nanoparticles were prepared by the reverse micelle method[15,16] in a procedure that involved preparation of two microemulsion systems. The first system consisted of an oil-phase microemulsion containing 108 mL of iso-octane and 24 g of surfactant diiso-octylsulphoccinate (AOT) and the second was an aqueous phase emulsion consisting of iso-octane and surfactant AOT with the reactant salts (hydrated iron chloride and hydrated nickel chloride). Microemulsion system I consisted of 2 mL of 30% NH_4OH + 2.4 mL of water + 66 mL of 0.50 M AOT-iso-octane and sonicated for 10 min. Microemulsion system II contained 0.275 g of $FeCl_2.4H_2O$ and 0.164 g of $NiCl_2.6H_2O$ dissolved in 8 mL of water + 66 mL of AOT-iso-octane and sonicated for 10 min. In microemulsion I, NH_4OH was the precipitating agent. On subjecting the two microemulsions to rapid mechanical stirring for 75 min., the metal hydroxides were precipitated within the water pools of reverse micelles and oxidized to ferrite. The precipitation of $NiFe_2O_4$ occurred according to the following reaction:

$$NiCl_2.6H_2O + 2FeCl_2.4H_2O + 6NH_4OH + \tfrac{1}{2}\,O_2 \rightarrow NiFe_2O_4 \downarrow + 6NH_4Cl + 17H_2O$$

Thus, these nanocrystalline nickel ferrites in the microemulsion constituted the core of the composite nanoparticles.

The second part of the process was initiated by introducing an aqueous solution of acidic titanium salt solution into the nickel ferrite product microemulsion. This leads to the following chemical reaction:

$$TiCl_4 + H_2O \rightarrow TiOCl_2 + 2HCl$$

The amount of $TiCl_4$ (0.08 mL $TiCl_4$) added was in accordance with the molar ratio of 1:1 in the TiO_2-$NiFe_2O_4$ system. This was followed by heating the nickel ferrite microemulsion containing acidic titanium salt solution at 90°C to precipitate titania on the surface of nickel ferrite particles. The solid product was separated by centrifuging at a speed of 15,000 rpm, washed a number of times with methanol and distilled water, and dried in an oven at 90°C for 30 min. The details of the process are summarized in Figure A.

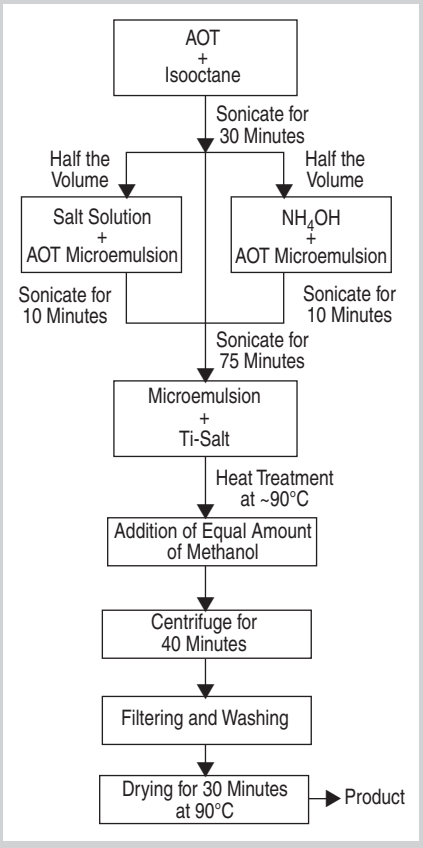

Figure A. A schematic flow sheet for the synthesis of TiO_2-$NiFe_2O_4$ composite nanoparticles by a combination of reverse micelle and chemical hydrolysis.

Structural and Magnetic Characterization

The TiO_2-$NiFe_2O_4$ composite nanoparticles were characterized by transmission-electron microscopy and x-ray diffraction techniques. X-ray diffraction studies were carried out using CuKα radiation of wavelength λ = 0.1540 nm. The magnetic properties were examined by a superconducting quantum interference device magnetometer in terms of the effect of temperature on magnetization and applied field on magnetization. Two methods for magnetization measurements were used, namely zero-field-cooling (ZFC) and field cooling (FC). In

Magnetic Properties of TiO_2-$NiFe_2O_4$ Nanoparticles

Representative zero-field-cooled (ZFC) and field-cooled (FC) saturation magnetization plots obtained for the TiO_2-$NiFe_2O_4$ system at an applied field of 2 kOe using a superconducting quantum interference device are presented in Figure 2. As shown in the inset of Figure 2, the magnetization-versus-temperature plot exhibits a feeble cusp in the ZFC magnetization at ~8 K, referred to as T_{max}. At temperatures above T_{max}, the FC plot diverges from the ZFC plot. The separation between the ZFC and the FC plots, even though small, gives an indication that there is a non-equilibrium magnetization state below ~18 K for the ZFC case, and represents the irreversibility temperature, T_{irr}.[18] In general, T_{irr} represents the blocking temperature of particles with the highest energy barrier and T_{max} is related to the average blocking temperature. The difference between T_{max} and T_{irr} corresponds to the width of the blocking temperature distribution. The T_{max} and T_{irr} temperatures are not too dissimilar from those obtained for uncoated nanocrystalline nickel ferrite (Table II).[16]

A variation of magnetization with the applied field at a temperature of 300 K is presented in Figure 3, where an absence of hysteresis, almost immeasurable coercivity and remanence, and the non-attainment of saturation even at a high magnetic field of 50 kOe are observed. The non-saturation of the M-H loop and the absence of hysteresis and coercivity at 300 K is indicative of the presence of superparamagnetic nature of the TiO_2:$NiFe_2O_4$ composite nanoparticles. Similar superparamagnetic behavior was observed for uncoated nanocrystalline nickel ferrite.[16]

Variations of magnetization with the applied field at a temperature of 2 K ($T<T_B$) for the TiO_2-$NiFe_2O_4$ composite nanoparticles is presented in Figure 3. Below the blocking temperature, the TiO_2-$NiFe_2O_4$ composite nanoparticles indicated a remanent magnetization and coercivity and exhibited a hysteretic feature. The particles do not have adequate thermal energy to attain complete thermal equilibrium with the applied field during the measurement time, and hysteresis appears. The remanent magnetization, coercivity, and saturation magnetization at 2 K are 1.3 emu/g, 0.55 kOe, and 15.5 emu/g, respectively. The lower value of magnetization for TiO_2-$NiFe_2O_4$ composite nanoparticles is related to two factors: the mass of $NiFe_2O_4$ in the TiO_2-$NiFe_2O_4$ samples and the size of the magnetic core of the coated particles, which is smaller compared to the uncoated nanoparticles. The

ZFC measurements, the sample was first cooled to 2 K in the absence of magnetic field, followed by magnetization measurements in the temperature range of 2 K to 300 K at an applied magnetic field of 2,000 Oe. In the FC-magnetization measurement, the sample was cooled to 2 K in the presence of an applied magnetic field, followed by magnetic measurements.

Photocatalytic Degradation of Methyl-Orange Dye

A cylindrical 250 mL pyrex glass bottle consisting of three parts was used for the degradation of methyl-orange dye experiment. The first, upper section allowed inlet and outlet gases, while the second and third sections enabled sampling and temperature measurements, respectively. The reactant suspension consisted of 0.001 g methyl-orange (concentration 0.008 g/L), 0.1 g catalyst (TiO_2:$NiFe_2O_4$), and 125 mL deionized water. The resulting aqueous suspension containing the methyl-orange and the catalyst powder was stirred and saturated by bubbling oxygen at atmospheric pressure with the lamp switched off. After about 20 min. the lamp was switched on for the initiation of reaction. During the reaction process, oxygen was continuously bubbled so that the steady state was maintained and the concentration of dissolved oxygen was not altered. To monitor the degradation, 4 mL of sample was removed at regular time intervals and filtered to separate the catalyst. The concentration of the unreacted methyl-orange was determined by ultraviolet spectrophotometer (JASCO, V550). The unreacted concentration was determined using Beer-Lambert Law, $A = \varepsilon cl$, where A is the absorbance at sample concentration c, l is the path length of quartz cell, and ε is molar absorptivity.

Anti-Microbial Activity of TiO_2-$NiFe_2O_4$ Composite Nanoparticles

A Luria-Bertani broth culture medium was prepared by dissolving 10 g Tryptone + 5 g NaCl + 5 g yeast extract in 1,000 mL distilled water, followed by sterilization in an autoclave at 121°C. A Luria-Bertani agar plate was prepared separately by dissolving 10 g tryptone + 5 g NaCl + 5 g yeast extract + 15 g agar in 1,000 mL distilled water. The solution was sterilized in an autoclave and poured into petri dish. E. coli k-12 (ATCC 29181) bacteria were grown in 100 mL conical flasks containing 10 mL of Luria-Bertani broth at 37°C on a rotatory shaker for 20 h. The speed of the shaker was set at 200 rpm. To provide fresh culture for the following experiments, aliquots of 10 µL of E. coli culture were transferred to a test tube containing 10 mL of Luria-Bertani broth. At this stage, the order of E. coli dilution was 10^{-3} in the broth. From this dilution, 10^{-7} dilution of E. coli in the Luria-Bertani broth was prepared. The cell concentration was determined by a viable count method on Luria-Bertani agar plates after 10^{-7} dilution of the culture in Luria-Bertani broth. Solutions of 10 µL and 100 µL were taken from the 10^{-7} dilution and spread on the Luria-Bertani agar plates. The plates were incubated at 37°C for 24 h prior to enumeration.

To study the photochemical reactivity of TiO_2-$NiFe_2O_4$ composite nanoparticles, two suspensions were prepared. The first suspension was an aqueous suspension of the composite nanoparticles (1 mg/mL in sterilized water). The second suspension was 10 µL of E. coli cells (~10^8 cfu/mL) suspended in 1 mL Luria-Bertani broth solution. Aliquots of 1 mL of composite nanoparticles from suspension I and suspension II were added to a 4 mL quartz cubic cell containing 1 mL of sterilized water. The resultant TiO_2-$NiFe_2O_4$ – E. coli cell slurry was placed in the UV spectrophotometer chamber (JASCO, V550) and irradiated with UV light (wavelength = 270 nm) for different periods of time. To determine the effectiveness of UV light in destroying bacteria, samples were taken out after different periods of UV light exposure. After irradiation for different time interval experiments, aliquots of 100 µL irradiated solution was transferred to a test tube containing 10 mL of Luria Bertani broth. The order of E. coli dilution at this stage is 10^{-2} in the Luria-Bertani broth. From the 10^{-2} dilution, serial dilutions of 10^{-3}, 10^{-4}, and 10^{-5} in the Luria-Bertani broth were prepared. The loss of viability for each exposure time was determined by the viable count procedure on Luria-Bertani agar plates after serial dilutions (10^{-2}, 10^{-3}, 10^{-4}, and 10^{-5}) of the irradiated solution in Luria-Bertani broth. 10 µL and 100 µL solutions were taken from the each dilution and spread on the Luria-Bertani agar plates. All the plates were incubated at 37°C for 24 h prior to enumeration. A similar procedure was conducted in the absence of TiO_2-$NiFe_2O_4$ composite nanoparticles.

Table I. A Comparison of Experimental and Standard Interplanar Spacing (d) Values with their Respective (h k l) Planes in TiO_2:$NiFe_2O_4$ Composite Nanoparticles

Phase	d (nm) Experimental	d (nm) Standard[17]	Diffraction Plane (h k l)
$NiFe_2O_4$ (cubic spinel)	0.2945	0.2950	2 2 0
	0.2520	0.2510	3 1 1
	0.2055	0.2080	4 0 0
	0.1450	0.1480	4 4 0
	0.1235	0.1270	5 3 3
TiO_2 (anatase phase, tetragonal)	0.3520	0.3520	1 0 1
	0.2374	0.2370	1 0 3
	0.1450	0.1480	2 1 3
	0.1235	0.1260	1 0 7

Table II. A Comparison of Magnetic Properties of Uncoated $NiFe_2O_4$ and Anatase TiO_2-Coated $NiFe_2O_4$ Nanoparticles

Sample	T_{max} (K)	T_{irr} (K)	Saturation Magnetization (emu/g) 2 K	Saturation Magnetization (emu/g) 300 K	Coercivity 2 K (kOe)	Remanence 2 K (emu/g)
$NiFe_2O_4$[16]	16.0	40.0	35.5	25.4	0.40	8.8
Anatase TiO_2-Coated $NiFe_2O_4$	8.0	18.0	15.5	3.8	0.55	1.3

uncoated particle had a size of 7–10 nm, while the coated nanoparticles had a core size of ~4–6 nm.

Photocatalytic Properties of TiO_2-$NiFe_2O_4$ Composite Nanoparticles

When a UV photon is absorbed by a TiO_2 particle, an e^-/h^+ pair is generated according to Equation 1. At the TiO_2 particle surface, the holes react with surface hydroxyl groups (OH^-) and adsorbed H_2O to form hydroxyl radicals ($^\bullet OH$). Photocatalytic reaction is based on the generation of very active $^\bullet OH$ mainly obtained according to Equations 2, 3, and 5.

$$TiO_2 + h\nu \rightarrow h^+ + e^- \quad (1)$$

$$OH^- + h^+ \rightarrow {}^\bullet OH \quad (2)$$

$$H_2O + h^+ \rightarrow {}^\bullet OH + H^+ \quad (3)$$

The presence of oxygen prevents this recombination by trapping electrons through the formation of superoxide ions ($O_2^{\bullet -}$) according to Equation 4. The final product of the reduction may also be $^\bullet OH$ radical.

$$O_2 + e^- \rightarrow O_2^{\bullet -} \quad (4)$$

$$2\,O_2^{\bullet -} + 2H^+ \rightarrow 2\,{}^\bullet OH \quad (5)$$

The photocatalytic decomposition process is effective in the destruction of chromophoric structures of dyes, and removing color that is the main undesirable factor for water recycling.[19,20] Methyl-orange is an acid-base indicator and is considered a model of a series of common azo-dyes used in the industry. The photocatalytic response of TiO_2-$NiFe_2O_4$ composite nanoparticles in the degradation of methyl-orange is presented in Figure 4. The methyl-orange photodegraded as irradiation time increased. Figure 4 shows that the methyl-orange concentrations are inversely proportional to the reaction time and the concentration was decreased from ~25 to ~4 μmol on irradiation for 7 h. Figure 4 also suggests that the primary degradation follows zero order kinetics, and can be expressed by:

$$[C_0] - [C] = kt \quad (6)$$

where C_0 is the initial concentration of the methyl-orange, C is the concentration of the methyl-orange at irradiation time t, and k is a rate constant related to the reaction. The rate constant k derived from Figure 4 is ~4.4×10^{-2} μmol/min.

Anti-Microbial Activity of TiO_2-$NiFe_2O_4$ Composite Nanoparticles

When TiO_2 powders (suspended in water) are irradiated with UV light, free ($^\bullet OH$) radicals are generated that are highly toxic toward the microorganism. This idea has been explored to investigate the E. coli bacterial inactivation in Luria-Bertani culture medium in the presence of UV-irradiated TiO_2-$NiFe_2O_4$ composite nanoparticles. Figure 5 shows the effect of TiO_2- $NiFe_2O_4$ on bacterial inactivation or germicidal action in the presence of UV light. It is clear from Figure 5 that at a constant irradiation time both in the presence and absence of TiO_2-$NiFe_2O_4$, composite nanoparticles decrease the concentration of E. coli bacteria, but the decrease in concentration is more for a TiO_2-$NiFe_2O_4$ composite nanoparticle system compared to UV light alone.

The inactivation of bacteria by UV irradiation results primarily from the UV absorption by DNA of the micro-

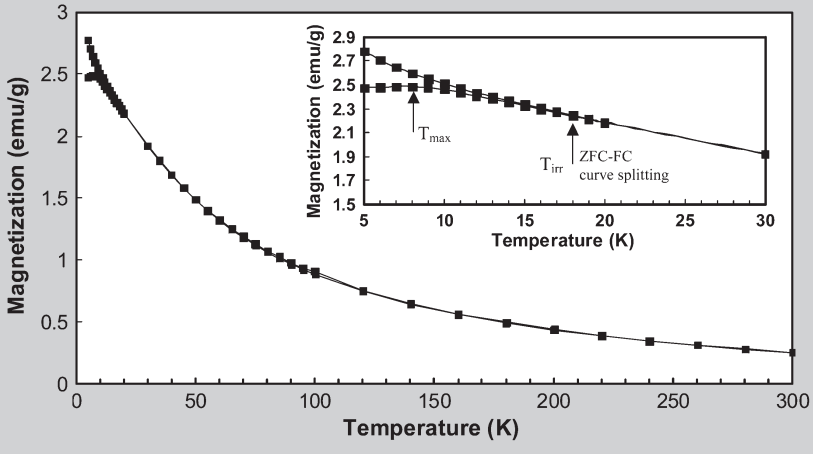

Figure 2. The variation of magnetization with temperature of TiO_2-$NiFe_2O_4$ composite nanoparticles at an applied field of 2 kOe. The inset is the part of the curve at lower temperatures and shows the blocking temperature distribution and the ZFC-FC curve splitting.

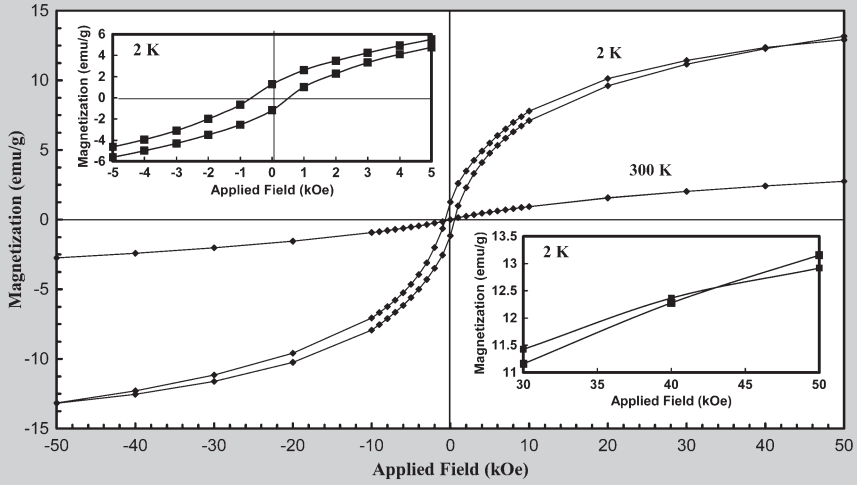

Figure 3. The variation of magnetization of TiO_2-$NiFe_2O_4$ composite nanoparticles with the applied field at 300 K and 2 K. The inset on the top left corner is the part of the curve near the origin showing the remanence and coercivity. The inset on the lower right corner is the part of the curve at higher applied fields showing the open loop and non-attainment of saturation magnetization.

organism. During irradiation, bacterial chromosomes form thymine dimers, a cross-link between the thymine bases within the same strand of DNA. These thymine dimers obstruct the conformation of the double helix and interfere with normal DNA replication.[21] On the other hand, photocatalytic inactivation in the presence of TiO_2 can be explained in terms of the attack of $O_2^{\bullet -}$, $^{\bullet}HO_2$, and $^{\bullet}OH$ radicals photogenerated on the surface of the catalyst but the $^{\bullet}OH$ radical is the most effective. The $^{\bullet}OH$ radical can oxidize the organic compounds adsorbed on the semiconductor surface and inactive microorganisms in bacteria cell according to Equation 7.

$$\text{Bacteria} + {}^{\bullet}\text{OH} \rightarrow \text{Bacterial inactivation} \qquad (7)$$

Matsunaga et al.[9] suggested that the hole in the valence band receives an electron from coenzyme A (CoA) as the donor forming dimeric CoA. Dimerization of CoA inhibits respiration and causes the death of the cells. More recently, Maness et al.[22] reported that in the presence of TiO_2, the lipid peroxidation reaction takes place. Consequently, the normal functions associated with an intact membrane, such as respiratory activity, are lost.

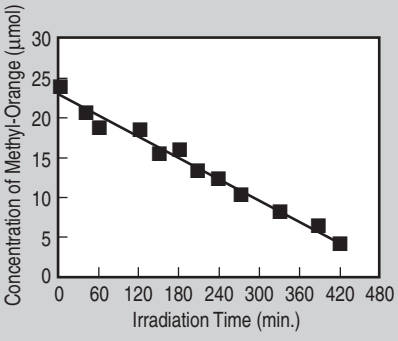

Figure 4. The concentration of methyl-orange versus irradiation time in the presence of TiO_2-$NiFe_2O_4$ composite nanoparticles.

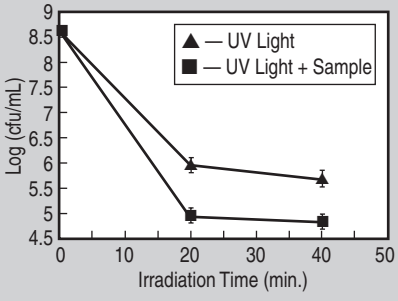

Figure 5. The E. coli bacterial inactivation response of TiO_2-$NiFe_2O_4$ composite nanoparticles as a function of irradiation time.

CONCLUSIONS

Composite nanoparticles characterized by a photocatalytic shell of anatase-titania and a magnetic core of nickel ferrite have been fabricated by combining reverse micelle and chemical hydrolysis methods.

The TiO_2-$NiFe_2O_4$ composite nanoparticles retained the magnetic characteristics of uncoated nanocrystalline nickel ferrites. The retention of magnetic strength encourages their application as removable photocatalyst nanoparticles.

TiO_2-$NiFe_2O_4$ composite nanoparticles exhibit anti-microbial activity when exposed to UV light. Bacterial inactivation is more efficient in the presence of UV light and TiO_2-$NiFe_2O_4$ composite nanoparticles than UV light alone.

References

1. A. Fujishima and K. Honda, *Nature,* 238 (1972), p. 37.
2. M.A. Fox and M.T. Dulay, *Chem. Rev.,* 93 (1993), p. 341.
3. M.R. Hoffmann et al., *Chem. Rev.,* 95 (1995), p. 69.
4. D.F. Ollis and H. El-Akabi, editors, *Photocatalytic Purification and Treatment of Water and Air* (Amsterdam: Elsevier Science, 1993).
5. M. Adachi et al., *J. Electrochem. Soc.,* 150 (2003), p. G488.
6. A.G. Rincon et al., *J. Photochem. Photobiol. A: Chem.,* 139 (2001), p. 233.
7. K. Sunada, T. Watanabe, and K. Hashimoto, *J. Photochem. Photobiol. A: Chem.,* 156 (2003), p. 227.
8. R.J. Watts et al., *Water Research*, 29 (1995), p. 95.
9. T. Matsunaga et al., *Appl. Environ. Microbiol.,* 54 (1988), p. 1330.
10. T. Matsunaga and M. Okochi, *Environ. Sci. Technol.,* 29 (1995), p. 501.
11. F. Chen et al., *Chemosphere,* 44 (2001), p. 1159.
12. D. Beydoun and R. Amal, *Mater. Sci. Eng. B,* 94 (2002), p. 71.
13. D.G. Shchukin, A.I. Kulak, and D.V. Sviridov, *Photochem. Photobiol. Sci.,* 1 (2002), p. 742.
14. Y. Gao et al., *Mater. Chem. Phys.,* 80 (2003), p. 348.
15. R.D.K. Misra et al., *Mater. Sci. & Eng. B,* 111 (2004), p. 164.
16. S. Gubbala et al., *Physica B,* 348 (2004), p. 317.
17. W.F. McClume, editor, Joint Committee on Powder Diffraction Standards (Swarthmore, PA: International Center for Diffraction Data, 1979) X-ray powder JCPDS diffraction files (a) 03.0875, $NiFe_2O_4$ and (b) 01.0562, anatase TiO_2.
18. B. Martinez et al., *Phys. Rev. Lett.,* 80 (1998), p. 181.
19. G. Marci et al., *Annali Di Chimica,* 93 (2003), p. 639.
20. C.Y. Yun et al., *Water Sci., Technol.,* 49 (2004), p. 177.
21. G.D. Harris et al., *Water Resear.,* 21 (1987), p. 687.
22. P.C. Maness et al., *Appl. Environ. Microbiol.,* 65 (1999), p. 4094.

S. Rana and R.D.K. Misra are both with the Center for Structural and Functional Materials and the Department of Chemical Engineering at the University of Louisiana at Lafayette.

For more information, contact R.D.K. Misra, University of Louisiana at Lafayette, Center for Structural and Functional Materials, P.O. Box 44130, Lafayette, LA 70504-4130; (337) 482-6430; e-mail dmisra@louisiana.edu.